CELL BIOLOGY

Bimolecular complementation affinity purification (BiCAP) reveals dimer-specific protein interactions for ERBB2 dimers

David R. Croucher,[1,2,3]* Mary Iconomou,[1†] Jordan F. Hastings,[1†] Sean P. Kennedy,[1,4†] Jeremy Z. R. Han,[1] Robert F. Shearer,[1] Jessie McKenna,[1] Adrian Wan,[5] Joseph Lau,[5] Samuel Aparicio,[5,6] Darren N. Saunders[1,7]*

The dynamic assembly of multiprotein complexes is a central mechanism of many cell signaling pathways. This process is key to maintaining the spatiotemporal specificity required for an accurate, yet adaptive, response to rapidly changing cellular conditions. We describe a technique for the specific isolation and downstream proteomic characterization of any two interacting proteins, to the exclusion of their individual moieties and competing binding partners. We termed the approach bimolecular complementation affinity purification (BiCAP) because it combines the use of conformation-specific nanobodies with a protein-fragment complementation assay with affinity purification. Using BiCAP, we characterized the specific interactome of the epidermal growth factor receptor (EGFR) family member ERBB2 when in the form of a homodimer or when in the form of a heterodimer with either EGFR or ERBB3. We identified dimer-specific interaction patterns for key adaptor proteins and identified a number of previously unknown interacting partners. Functional analysis for one of these newly identified partners revealed a noncanonical mechanism of extracellular signal–regulated kinase (ERK) activation that is specific to the ERBB2:ERBB3 heterodimer and acts through the adaptor protein FAM59A in breast cancer cells.

INTRODUCTION

Intracellular signaling networks are the master regulators of processes such as mitosis, apoptosis, migration, and differentiation. Although the phosphorylation of kinase substrates can alter their activity, localization, or stability, the modulation of protein-protein interactions at these phosphorylation sites also serves as a major mechanism to maintain the specificity and dynamic properties of signaling pathways (*1*, *2*). Consequently, significant effort has been invested in developing techniques to identify and quantify protein-protein interactions relevant to cell signaling. Affinity purification coupled with tandem mass spectrometry (AP-MS/MS) has emerged as a powerful technology to characterize the interactome of any given protein. Although a number of seminal MS-based studies have greatly increased our understanding of the dynamic nature of protein-protein interactions (*3*–*5*), these approaches are often limited to the analysis of an individual protein in all potential binding states. Many proteins are activated or inhibited upon dimerization or complex formation, considerably altering the dynamics of a signaling pathway. It is therefore an experimental imperative that further techniques are developed, which can dissect these multiprotein complexes and characterize the specific function of each modular component within specific spatial and temporal contexts.

In response to this challenge, we developed a novel method for the specific isolation and characterization of the interactome of any binary protein complex. This approach combines a protein-fragment complementation assay and affinity purification with a conformation-specific nanobody, which we have termed bimolecular complementation affinity purification (BiCAP). This novel technique exploits a neoepitope formed by complementation of Venus fluorescent protein fragments to specifically isolate any pair of interacting proteins while excluding competing binding partners and those binding to individual components in isolation. A further advantage of this approach is the simultaneous visualization of cellular localization of interacting protein pairs. We have applied this approach to characterize the interactome of the receptor tyrosine kinase (RTK) oncogene ERBB2, which can exist as either a monomer, a homodimer, or a heterodimer with other members of the epidermal growth factor receptor (EGFR) family (*6*).

The formation of heterodimers within the EGFR family has long been thought to diversify the interactome and signaling capacity of these receptors when compared to receptor homodimers (*7*–*10*). In breast cancer cells where *ERBB2* is amplified, and therefore overexpressed, the formation of ERBB2-containing heterodimers can be driven in a ligand-independent manner (*8*, *11*). ERBB2 is the preferred dimerization partner for EGFR and ERBB3 (*12*), and the signals emanating from these heterodimers are known to be significantly stronger than those from other EGFR family receptor combinations (*6*). Each of these receptors is also a potent breast cancer oncogene and the target of multiple therapeutic agents (*6*, *8*). Despite promising initial results in clinical trials, acquired resistance frequently emerges with both antibody and small-molecule therapies directed toward these EGFR family members (*13*). A shift in the dimerization profile of ERBB2 is recognized as a common mechanism underlying resistance to ERBB2-targeting therapies (*13*, *14*), although this plasticity of ERBB2 also highlights a broader emerging theme in cancer research, where a thorough understanding of the dynamic and adaptable behavior of signaling networks will be required to ultimately deliver specific and efficient cancer therapies (*15*). To date, defining the specific interactomes of ERBB2-containing homo- and heterodimers has been hindered by

[1]The Kinghorn Cancer Centre, Garvan Institute of Medical Research, Sydney, New South Wales 2010, Australia. [2]St. Vincent's Hospital Clinical School, University of New South Wales, Sydney, New South Wales 2052, Australia. [3]School of Medicine, University College Dublin, Belfield, Dublin D4, Ireland. [4]Systems Biology Ireland, University College Dublin, Belfield, Dublin D4, Ireland. [5]Department of Molecular Oncology, British Columbia Cancer Research Centre, Vancouver, British Columbia V5Z 1L3, Canada. [6]Department of Pathology and Laboratory Medicine, University of British Columbia, Vancouver, British Columbia V6T 1Z4, Canada. [7]School of Medical Sciences, University of New South Wales, Sydney, New South Wales 2052, Australia.
*Corresponding author. Email: d.croucher@garvan.org.au (D.R.C.); d.saunders@unsw.edu.au (D.N.S.)
†These authors contributed equally to this work.

limitations on the ability to selectively purify receptor dimers while excluding individual monomers and alternative heterodimers. The application of BiCAP largely overcomes these limitations, facilitating characterization of the individual interactome of each of these ligand-independent receptor dimers.

RESULTS

Bimolecular fluorescence complementation for ERBB2 homodimers

Protein-fragment complementation assays are frequently used to visualize and quantify the interaction between two proteins in live cells. This technique relies upon the expression of bait and prey proteins fused to split domains of a reporter such as luciferase (*16*), β-galactosidase (*17*), or green fluorescent protein (GFP) (*18*). Interaction between bait and prey proteins drives refolding of the fused fragments into a functional reporter protein, generating a measurable signal. In the case of a protein-fragment complementation assay based on a split fluorescent protein such as GFP (or its variants), the term bimolecular fluorescence complementation (BiFC) is frequently used (*19*). The individual N- and C-terminal fragments of the GFP family proteins are nonfluorescent and associate with low affinity in the absence of an interaction between fusion partners. However, their close colocalization upon interaction of bait and prey fusion proteins favors refolding of these split domains into a functional β-barrel structure containing the fluorophore (*18*). This is demonstrated using a well-described homodimer formed by ERBB2. We engineered C-terminal fusions of ERBB2 with complementary BiFC fragments comprising either the N-terminal (Met^{1}-Gln^{157}) or C-terminal (Lys^{158}-Lys^{238}) regions of the Venus fluorescent protein, which is an engineered derivative of GFP. These vectors were termed ERBB2-V1 and ERBB2-V2, respectively (Fig. 1A). Transfection of plasmids encoding these individual fusion proteins into human embryonic kidney (HEK)–293T cells did not produce any fluorescent signal (fig. S1A). However, cotransfection of both plasmids generated a predominantly membranous fluorescent signal, as expected from the formation of an RTK dimer (Fig. 1B and fig. S1A). This transient transfection approach achieved an abundance of ERBB2 that was similar to that in ERBB2-amplified breast cancer cell lines AU565 and SKBR3 (fig. S1B).

Although BiFC enables the visualization of specific ERBB2 homodimers, the ability to isolate and characterize these dimers (while excluding nondimerized ERBB2 monomers and alternative heterodimers) using standard immunoprecipitation approaches is problematic. For example, whereas we

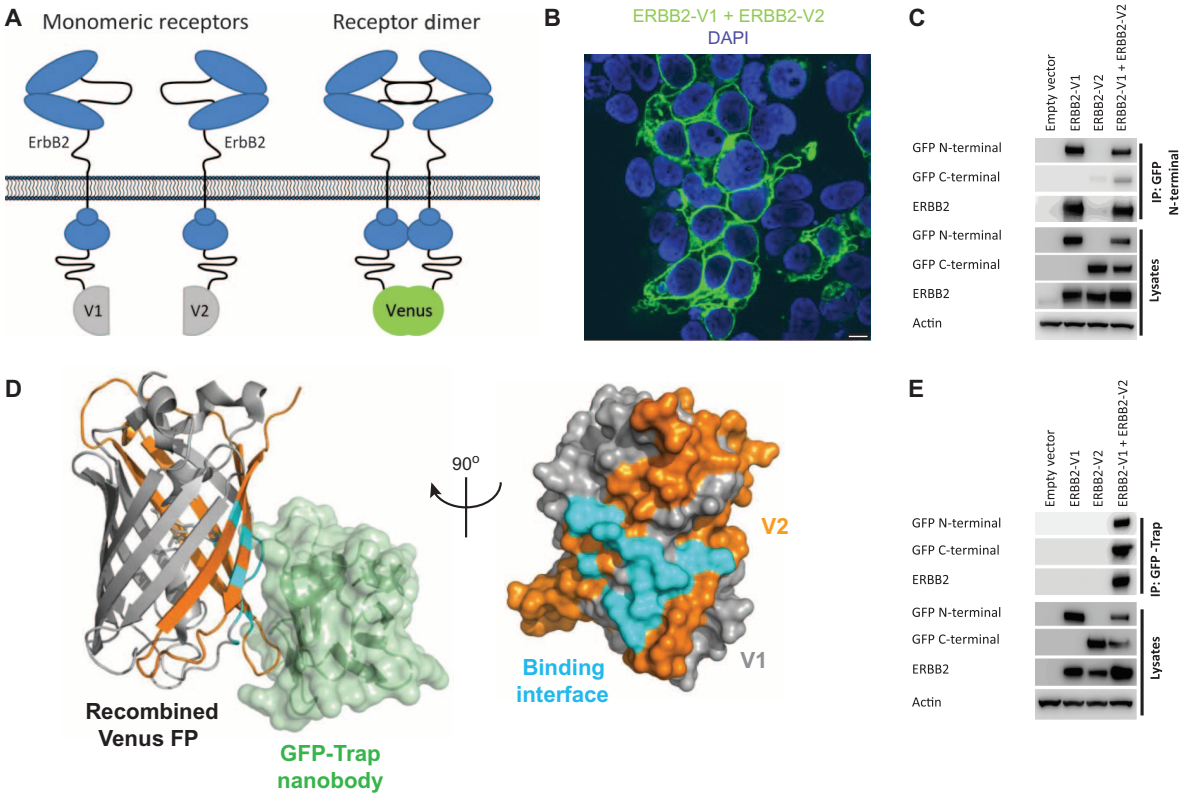

Fig. 1. Specific isolation of refolded bimolecular fluorescence complementation assay components. (**A**) Schematic depicting ERBB2 fused to nonfluorescent N-terminal (V1) and C-terminal (V2) fragments of the Venus protein, which refold and fluoresce upon interaction. (**B**) Confocal fluorescence microscopy analysis of BiFC signal produced by interaction between ERBB2-V1 and ERBB2-V2 after transfection into HEK-293T cells. Representative images from at least three independent experiments are shown. Scale bar, 7.5 μm. (**C**) HEK-293T cells were transfected with a control plasmid, ERBB2-V1, ERBB2-V2, or both ERBB2-V1 and ERBB2-V2, and then immunoprecipitation (IP) with antibodies against the N-terminal region of GFP (V1) and blotting with the indicated antibodies were performed on the cell lysates. Blots are representative of three experiments. (**D**) Structural analysis of the interaction interface (cyan) between GFP-targeting nanobody (GFP-Trap) (green) and recombined Venus, showing the position of Venus V1 (gray) and V2 (orange) fragments (Protein Data Bank accession 3OGO). (**E**) HEK-293T cells were transfected as in (C), followed by immunoprecipitation with GFP-Trap and blotting with the indicated antibodies. Blots are representative of three experiments.

observed about equal expression of ERBB2-V1 and ERBB2-V2 after cotransfection of HEK-293T cells, a higher proportion of ERBB2-V1 than ERBB2-V2 was detected after immunoprecipitation using an antibody raised against the N-terminal region of GFP (Fig. 1C). Hence, this approach is not able to adequately enrich for ERBB2 dimers as a fraction of the total ERBB2 population, and the greater presence of ERBB2 monomers or heterodimers would confound attempts to characterize ERBB2 dimer–specific interactomes and signaling complexes. Thus, a more elegant approach is needed to facilitate the specific isolation and characterization of ERBB2 binary protein complexes.

Bimolecular complementation affinity purification

Analysis of the binding epitope of a GFP-Trap (*20*) suggested that it may provide a suitable affinity purification matrix for specific enrichment of ERBB2 BiFC dimers while excluding monomeric ERBB2. GFP-Trap is a recombinant antibody fragment (nanobody) that binds with high affinity to GFP and its derivatives (YFP, CFP, Venus, Citrine, and AcGFP) (*20*). GFP-Trap recognizes a three-dimensional epitope on the β barrel of GFP created by noncontiguous amino acid sequences. Closer analysis of this binding epitope showed that it spans a surface of the fluorescent protein β barrel, which is composed of both the V1 and V2 BiFC fragments (Fig. 1D). This suggests that GFP-Trap recognizes a neoepitope that exists on correctly recombined and folded Venus but that does not exist on the individual BiFC fragments. Hence, we hypothesized that GFP-Trap would bind specifically to recombined Venus but not to the individual Venus fragments used for BiFC.

We tested the ability of GFP-Trap to specifically enrich for ERBB2 dimers after cotransfection of HEK-293T cells with ERBB2-V1 and ERBB2-V2. The presence of both ERBB2-V1 and ERBB2-V2 in GFP-Trap eluate from cotransfected cells, but not from cells transfected with either ERBB2-V1 or ERBB2-V2 alone (Fig. 1E), demonstrates that GFP-Trap specifically isolated the ERBB2 homodimer but was unable to bind ERBB2-V1 or ERBB2-V2 in isolation. This unique combination of a protein-fragment complementation assay with a conformation-specific nanobody therefore provides a powerful method to isolate protein complexes while excluding the uncomplexed individual components and competing binding partners. A further advantage of this system is the ability to visualize protein interactions in situ, providing confirmation of cellular context. We have termed this novel technique BiCAP.

Characterization of dimer-specific ERBB2 interactomes by BiCAP

BiFC has previously been used to visualize the formation of EGFR family dimers (*21*), but here, we sought to demonstrate the utility of the BiCAP approach by applying it to characterize the specific interactomes of ERBB2 homodimers or ERBB2 heterodimers with EGFR or ERBB3 (Fig. 2A). Expression of individual heterodimer components was confirmed by Western blotting cell lysates from HEK-293T cells cotransfected with BiFC-tagged receptor pairs (Fig. 2B). A prominent membranous fluorescent signal was observed for each dimer, indicating the formation of plasma membrane–localized receptor dimers (Fig. 2C). Notably, ERBB3:ERBB2 dimers also displayed a distinct perinuclear signal. Label-free quantitative MS analysis of BiCAP-isolated receptor dimers (Fig. 2D) revealed distinct interactomes for each dimer pair (Table 1). Analysis of known protein-protein interactions using the String database (*22*) highlighted the existence of a number of established functional clusters in the individual interactome of each receptor dimer (Fig. 2E). A prominent core group of 10 proteins was observed in the interactome of all three receptor dimers (Fig. 3). This core interactome contains many established components of RTK signaling pathways, including the adaptor proteins GRB2 and SHC1, known to interact with various activated RTKs and activate RAS signaling (*23*, *24*) through the guanine nucleotide exchange factor (GEF) Son of Sevenless homolog 1 (SOS1) (*25*). ERBB receptor feedback inhibitor 1 (ERRFI1), otherwise known as mitogen-inducible gene 6 (MIG6), is known to interact with and inhibit the kinase domains of EGFR family members (*26*–*28*), whereas the GEFs VAV2 and VAV3 are established links between EGFR family members and guanosine triphosphatase activation (*29*, *30*).

A small group of proteins were detected interacting exclusively with ERBB2 homodimers, consisting of transferrin receptor (TFRC), endoplasmic reticulum lipid raft associated 1 (ERLIN1), and protein tyrosine phosphatase nonreceptor type 9 (PTPN9). ERBB2 is a substrate of PTPN9, which attenuates activation of signal transducer and activator of transcription proteins downstream of ERBB2 (*31*). Although the specific function of the ERLIN1 and TFRC interactions is not yet known, the presence of these may be suggestive of the localization of ERBB2 homodimers within lipid rafts and recycling endosomes, respectively (*32*). Another small group of proteins interacted exclusively with the EGFR:ERBB2 heterodimer. These include the E3-ligase c-Cbl, which ubiquitinates activated EGFR to promote its degradation (*33*), and phospholipase C γ1 (PLCG1), which drives the activation of protein kinase C (PKC) after binding to activated EGFR (*34*). Only three proteins were observed to interact specifically with both ERBB2 homodimers and EGFR:ERBB2 heterodimers: ubiquitin-associated and Src homology 3 (SH3) domain–containing B (UBASH3B), SOS2, and ERBB4. UBASH3B interferes with Cbl-mediated degradation of activated EGFR (*35*), which may indicate increased stability of the EGFR:ERBB2 dimer (*32*), although the interaction of these dimers with ERBB4 may also indicate potential formation of higher-order receptor complexes within the EGFR family (*36*, *37*).

As may be expected, a number of interacting proteins play a role in the endocytosis, sorting, and recycling of RTKs. For example, CHMP5, which interacted with EGFR:ERBB2, is a component of the endosomal sorting complex required for transport III (ESCRT-III) and plays an essential role in trafficking and degradation of growth factor receptors (*38*). The clathrin adaptor proteins AP2M1 and AP1M1, which were present in complex with both the EGFR:ERBB2 and ERBB3:ERBB2 heterodimers, bind to transmembrane cargo proteins and thus play a major role in trafficking via clathrin-coated vesicles. The absence of these trafficking-related proteins from the ERBB2 homodimer is in keeping with the concept that ERBB2, unlike EGFR and ERBB3, may have an impaired ability to undergo endocytosis due to a lack of C-terminal internalization signals (*32*).

By far, the largest group of proteins, representing a diverse group of 44 proteins, was found to interact exclusively with ERBB3:ERBB2 heterodimers. Many of these proteins are associated with the ribosome or RNA binding and splicing (RBMX, RAE1, EIF3B, STAU1, PRKRA, RSL1D1, HNRNPC, SNRPD1, SRSF5, HNRNPA0, RPF2, PABPN1, RBM34, ELAVL1, RRS1, LTV1, U2AF2, and BRIX1) or to have a role within the nucleus (NOP2, TPR, RANBP2, LYAR, EBNA1BP2, and SAFB). There was also a large group of mitochondrial proteins (MRPS22, MRPS34, AIFM1, MRPS16, MRPS5, MRPS26, MRPS25, MRPS18B, and MRPS9). Smaller groups of proteins were also identified with more specialized roles as either cytoskeletal/structural proteins (SPTAN1, INA, and DSG2), transcription factors (TP53 and NKRF), or signaling pathway components (FAM59A, PIK3R2, GNAI1, and PLCG2).

Within this system, the expanded interactome of ERBB3:ERBB2 may potentially be influenced by the distinct intracellular localization of this heterodimer (Fig. 2A). Observations of intracellular ERBB3 are not uncommon, including the detection of functional ERBB3:ERBB2 heterodimers in the nucleus (*39*–*42*). Therefore, the intracellular localization of ERBB3:ERBB2 heterodimers within this BiFC system does not appear to be an artefact of transfection because this localization is also consistent with that

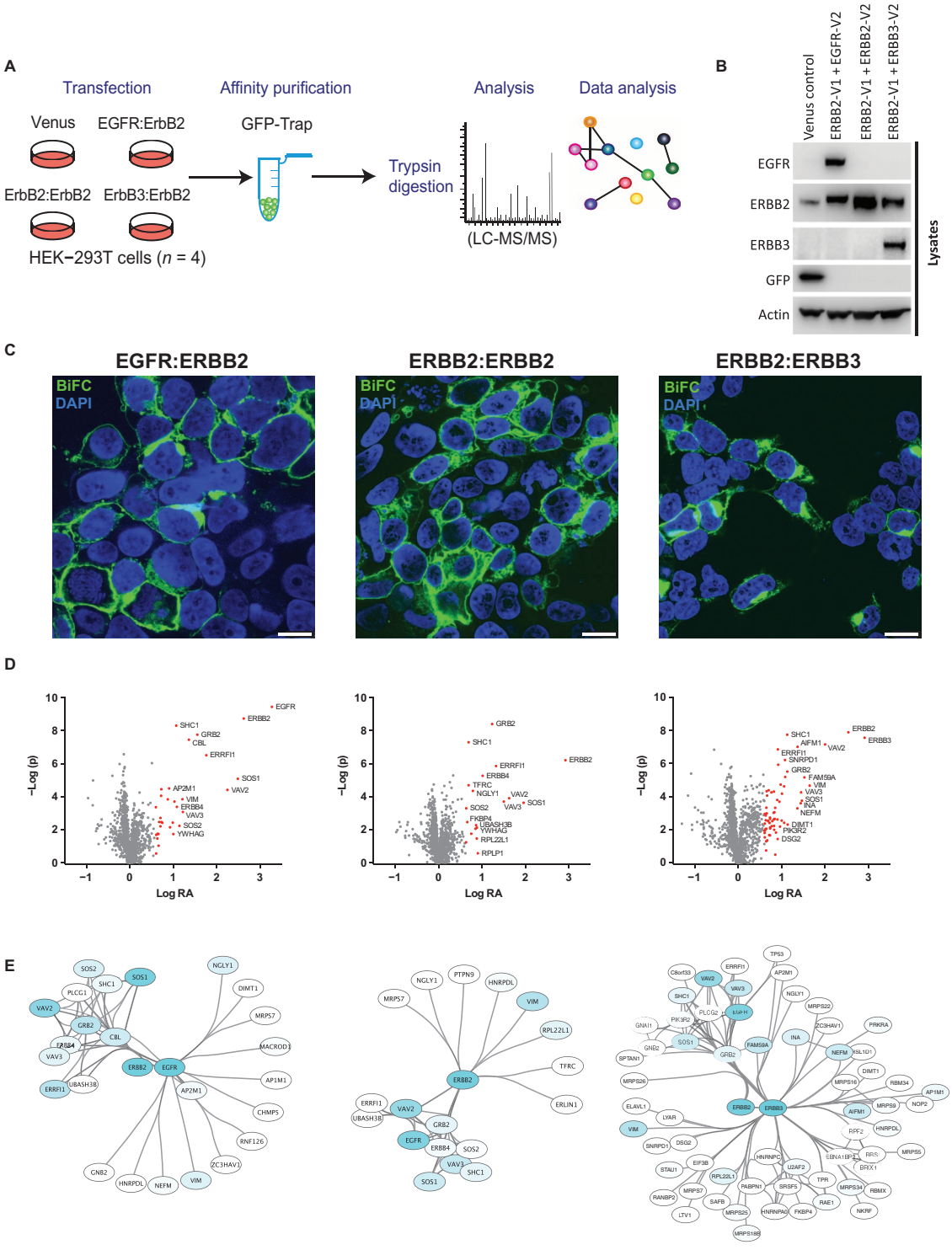

Fig. 2. MS analysis of proteins interacting with specific ERBB2-containing dimers. (**A**) Workflow for the isolation and MS analysis of specific ERBB2-containing receptor dimers. (**B**) HEK-293T cells were transfected with either a control plasmid or a combination of ERBB2-V1 and either EGFR-V2, ERBB2-V2, or ERBB3-V2, with expression confirmed by blotting lysates with the indicated antibodies. Blots are representative of three experiments. (**C**) Confocal fluorescence microscopy analysis of BiFC signal produced by interaction between ERBB2-V1 and either EGFR-V2, ERBB2-V2, or ERBB3-V2, after transfection into HEK-293T cells. Representative images from at least three independent experiments are shown. Scale bars, 15 μm. (**D**) Protein interaction networks of the ERBB2: ERBB2 homodimer, EGFR:ERBB2 heterodimer, or ERBB3:ERBB2 heterodimer with relative abundance of individual components indicated by cyan shading (darker means more abundant). LC-MS/MS, liquid chromatography–MS/MS; DAPI, 4′,6-diamidino-2-phenylindole.

Table 1. Label-free quantitative proteomics analysis of ERBB2 dimer interactomes isolated by BiCAP. The table shows the 15 most abundant proteins in each complex. Complete list is in table S3. Unique peptides are the total number of unique peptides associated with the protein group (that is, not shared with another protein group). Unique sequence coverage (%) is the percentage of the sequence that is covered by the identified peptides of the best protein sequence contained in the group. PEP, posterior error probability (posterior error probability of the identification, smaller values are more significant); *Q*, Benjamini-Hochberg false discovery rate (FDR)– adjusted *P* value (FDR < 0.1).

Bait	UniProt ID	Gene ID	Protein name	Unique peptides	Unique (%)	*P* (*t* test)	*Q*	Relative abundance
ERBB2:ERBB2	P04626	ERBB2	Receptor tyrosine-protein kinase erbB-2	62	52.4	6.16×10^{-7}	1.72×10^{-4}	835.1
	G5E9C8	SOS1	Son of sevenless homolog 1	53	47.9	2.18×10^{-4}	9.47×10^{-3}	89.3
	P52735-3	VAV2	Guanine nucleotide exchange factor VAV2	33	44.8	4.85×10^{-5}	4.22×10^{-3}	37.5
	Q9UKW4	VAV3	Guanine nucleotide exchange factor VAV3	23	35.4	9.36×10^{-5}	6.52×10^{-3}	28.5
	Q9UJM3	ERRFI1	ERBB receptor feedback inhibitor 1	12	39	2.56×10^{-7}	9.18×10^{-5}	20.0
	P62993	GRB2	Growth factor receptor–bound protein 2	23	86.6	3.97×10^{-9}	5.53×10^{-6}	17.1
	Q15303	ERBB4	Receptor tyrosine-protein kinase erbB-4	3	2.2	1.80×10^{-6}	3.57×10^{-4}	10.4
	Q96IV0	NGLY1	Peptide-*N*(4)-(*N*-acetyl-β-glucosaminyl)asparagine amidase	9	19.1	3.02×10^{-4}	1.05×10^{-2}	9.1
	Q07890	SOS2	Son of sevenless homolog 2	9	8.6	8.45×10^{-7}	1.96×10^{-4}	8.7
	Q8TF42	UBASH3B	Ubiquitin-associated and SH3 domain–containing protein B	4	9.2	2.32×10^{-2}	8.31×10^{-2}	7.1
	P08670	VIM	Vimentin	59	77.9	8.82×10^{-3}	5.44×10^{-2}	7.1
	H0Y8C2	RPL22L1	60*S* ribosomal protein L22-like 1	3	33.8	1.13×10^{-2}	5.96×10^{-2}	6.8
	J3QLS3	MRPS7	28*S* ribosomal protein S7, mitochondrial	4	18.8	1.30×10^{-2}	6.35×10^{-2}	6.3
	P43378	PTPN9	Tyrosine-protein phosphatase nonreceptor type 9	2	4.7	3.30×10^{-2}	9.80×10^{-2}	5.2
	P29353-6	SHC1	SHC-transforming protein 1	6	7.5	5.01×10^{-8}	3.49×10^{-5}	4.9
ERBB2:EGFR	P00533	EGFR	Epidermal growth factor receptor	67	52.5	3.59×10^{-10}	5.00×10^{-7}	1881.2
	P04626	ERBB2	Receptor tyrosine-protein kinase erbB-2	62	52.4	1.82×10^{-9}	1.27×10^{-6}	421.7
	G5E9C8	SOS1	Son of sevenless homolog 1	53	47.9	6.42×10^{-6}	5.97×10^{-4}	299.2
	P52735-3	VAV2	Guanine nucleotide exchange factor VAV2	33	44.8	1.92×10^{-6}	2.43×10^{-4}	137.3
	Q9UJM3	ERRFI1	ERBB receptor feedback inhibitor 1	12	39	9.76×10^{-6}	7.86×10^{-4}	39.7
	P62993	GRB2	Growth factor receptor–bound protein 2	23	86.6	1.76×10^{-8}	6.13×10^{-6}	35.8
	P22681	CBL	E3 ubiquitin-protein ligase CBL	9	13.9	3.51×10^{-8}	9.78×10^{-6}	22.9
	Q07890	SOS2	Son of sevenless homolog 2	9	8.6	2.35×10^{-3}	2.01×10^{-2}	18.5
	Q96IV0	NGLY1	Peptide-*N*(4)-(*N*-acetyl-β-glucosaminyl)asparagine amidase	9	19.1	2.25×10^{-5}	1.32×10^{-3}	17.1
	P08670	VIM	Vimentin	59	77.9	1.42×10^{-4}	4.20×10^{-3}	16.4
	Q9UKW4	VAV3	Guanine nucleotide exchange factor VAV3	23	35.4	6.15×10^{-3}	3.13×10^{-2}	14.9
	P29353-6	SHC1	SHC-transforming protein 1	6	7.5	4.90×10^{-9}	2.27×10^{-6}	11.7
	Q15303	ERBB4	Receptor tyrosine-protein kinase erbB-4	3	2.2	1.72×10^{-3}	1.65×10^{-2}	11.7
	Q96CW1	AP2M1	AP-2 complex subunit mu	12	26.2	1.27×10^{-3}	1.41×10^{-2}	10.7
	P07197	NEFM	Neurofilament medium polypeptide	20	27.7	3.76×10^{-3}	2.48×10^{-2}	9.7
ERBB2:ERBB3	P21860	ERBB3	Receptor tyrosine-protein kinase erbB-3	69	53.9	2.69×10^{-8}	1.06×10^{-5}	814.8
	P04626	ERBB2	Receptor tyrosine-protein kinase erbB-2	62	52.4	1.26×10^{-8}	1.06×10^{-5}	344.3
	P52735-3	VAV2	Guanine nucleotide exchange factor VAV2	33	44.8	2.16×10^{-7}	3.82×10^{-5}	94.0
	P08670	VIM	Vimentin	59	77.9	2.14×10^{-5}	9.48×10^{-4}	44.2
	Q9H706	FAM59A	Protein FAM59A	9	15	1.50×10^{-7}	3.03×10^{-5}	28.1
	Q9UKW4	VAV3	Guanine nucleotide exchange factor VAV3	23	35.4	1.28×10^{-4}	2.00×10^{-3}	27.6
	O95831	AIFM1	Apoptosis-inducing factor 1, mitochondrial	16	40.9	9.63×10^{-8}	2.73×10^{-5}	23.2
	P07197	NEFM	Neurofilament medium polypeptide	20	27.7	5.15×10^{-4}	4.35×10^{-3}	23.1
	G5E9C8	SOS1	Son of sevenless homolog 1	53	47.9	3.31×10^{-5}	1.06×10^{-3}	23.1
	Q16352	INA	α-Internexin	9	23.4	1.12×10^{-3}	6.50×10^{-3}	17.0
	H0Y8C2	RPL22L1	60*S* ribosomal protein L22-like 1	3	33.8	1.38×10^{-5}	8.14×10^{-4}	14.5
	P62993	GRB2	Growth factor receptor–bound protein 2	23	86.6	3.05×10^{-6}	3.09×10^{-4}	13.5
	P29353-6	SHC1	SHC-transforming protein 1	6	7.5	1.78×10^{-8}	1.06×10^{-5}	13.4
	Q9BXS5-2	AP1M1	AP-1 complex subunit mu-1	19	51.3	2.41×10^{-5}	9.48×10^{-4}	11.4
	C9JJ19	MRPS34	28*S* ribosomal protein S34, mitochondrial	11	60.4	6.70×10^{-5}	1.34×10^{-3}	10.2

previously observed for endogenous ERBB3 in breast cancer cells (*41*). Costaining with an antibody toward the Golgi body marker GM-130 confirmed that a large proportion of the ERBB3:ERBB2 heterodimer colocalizes within the Golgi body, along with the plasma membrane and nucleus (fig. S2). Additionally, to confirm some of these new and unexpected hits, we further validated the interaction of ERBB3:ERBB2 with a mitochondrial associated protein (AIFM1) and an RNA nucleocytoplasmic shuttle protein (RAE1) in HEK-293T cells (fig. S3A). We also validated the interaction of these proteins with endogenous ERBB2 by using a proximity-mediated ligation assay (PLA) in the SKBR3 breast cancer cell line (fig. S3B).

Interactome diversity directs signaling pathway activity

Quantitative analysis revealed varying enrichment of individual proteins from the core interactome with each of the three ERBB2 receptor dimers

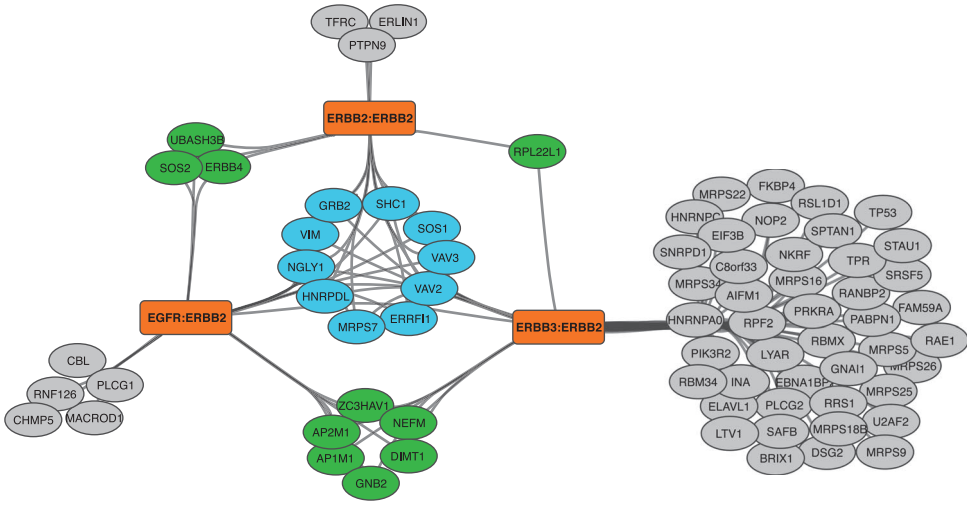

Fig. 3. Combined analysis of interactome diversity in ERBB2-containing dimers. Baits used for BiCAP are shown in orange, and core group of 10 proteins observed in the interactome of all three receptor dimers is shown in blue. Interacting proteins common to two receptor dimers are shown in green.

(Fig. 4A). Given the importance of protein-protein interactions in determining the specificity of pathway activation, it is likely that the observed diversity in the interactome of each receptor dimer may underlie their differential signaling potential. Taking the mitogen-activated protein kinase (MAPK) pathway components as an example, quantitative BiCAP data indicated that EGFR:ERBB2 dimers bound proportionally more GRB2, and therefore SOS, than did the other two dimers (Fig. 4B). In contrast, SHC binding was increased for both the EGFR:ERBB2 and ERBB3:ERBB2 heterodimers (Fig. 4B). In support of these MS-based observations, we also found that this pattern of interaction was recapitulated by Western blotting (Fig. 4C).

Previous studies into signaling pathway activation downstream of the EGFR family show that homodimers generally have weak signaling capacity (*6*, *8*) and that ERBB2-containing heterodimers elicit stronger signals than do other possible combinations (*6*). Consistent with these studies and the model of protein-protein interactions mediating signaling pathway activity, we observed significantly increased extracellular signal–regulated kinase (ERK) activation downstream of EGFR:ERBB2 and ERBB3:ERBB2 receptor heterodimers but not downstream of ERBB2 homodimers (Fig. 4D). This trend tends to more closely follow the strength of the SHC1 interaction rather than GRB2, in line with previous observations, suggesting that interaction with SHC1 is essential for MAPK pathway activation by ERBB3 (*43*). However, a further mechanism driving MAPK activation downstream of the ERBB3:ERBB2 dimer could also be the interaction with FAM59A, which is only observed for this specific heterodimer using BiCAP and Western blotting (Figs. 3 and 4, B and C). FAM59A, also known as GRB2-associated and regulator of ERK/MAPK (GAREM), is a recognized component of receptor-associated signaling complexes (*4*, *44*) and promotes ERK activation downstream of EGFR stimulation (*45*). FAM59A acts by binding to the SH3 domains of GRB2 and facilitates ERK activation in an SOS-independent manner (*45*). This mechanism is consistent with an absence of SOS1 or SOS2 in the interactome of ERBB3:ERBB2 heterodimers (Table 1 and Figs. 2D and 3), which nonetheless strongly activated ERK signaling (Fig. 4D).

FAM59A drives ERK activation by ERBB3:ERBB2 heterodimers

To investigate FAM59A-driven ERK activation from ERBB3:ERBB2 heterodimers in an endogenous setting, we performed Western blotting for FAM59A, EGFR, ERBB2, and ERBB3 in a panel of 25 breast cancer cell lines (Fig. 5A). As expected, EGFR was highest in basal breast cancer lines and ERBB2 was mostly restricted to clinically defined ERBB2$^+$ cell lines and some luminal lines, whereas ERBB3 was present mostly in luminal and ERBB2$^+$ lines. FAM59A is known to be ubiquitously expressed (*46*). Accordingly, FAM59A was present across all breast cancer subtypes, although slightly higher in basal lines. Therefore, FAM59A was present in all ERBB2/ERBB3-positive cell lines, although the increased FAM59A in basal breast cancer lines potentially indicates other signaling roles within these cells.

Although we could detect ERBB3:ERBB2 heterodimers by coimmunoprecipitation in four ERBB2$^+$ cell lines (fig. S4), this technique was unable to detect the interaction between this heterodimer and FAM59A. Therefore, to confirm that FAM59A interacts with ERBB2 in breast cancer cell lines, we used PLA, which has previously been used to visualize and quantify the interaction between GRB2 and EGFR (*47*). Using this technique, the interaction between ERBB2 and FAM59A could be observed in the ERBB2- and ERBB3-positive ZR75-30, SKBR3, and AU656 cell lines (Fig. 5B and fig. S5). Further investigation of this interaction in the MDA-MB-330 cell line (Fig. 5C) revealed that endogenous ERBB2 and ERBB3 were both localized in a punctate manner at the plasma membrane and in the cytoplasm, whereas endogenous FAM59A was also punctate but predominantly cytoplasmic. The dependency of the ERBB2-FAM59A interaction upon ERBB3:ERBB2 dimer formation was supported by analysis of the ERBB2-FAM59A PLA signal in MDA-MB-330 cells, where a significant decrease in PLA signal was observed in cells treated with ERBB3 siRNA compared to cells treated with control siRNA (Fig. 5C). The functional relevance of this signaling complex was highlighted by a significant reduction in ERK phosphorylation (Fig. 5D) and colony formation (Fig. 5E) after FAM59A knockdown in MDA-MB-330 cells. These results were also recapitulated in the SKBR3 cell line using two independent siRNAs against FAM59A (fig. S6).

Whereas FAM59A knockdown reduced ERK activation, ERBB3 knockdown reduced both ERK and AKT activation in MDA-MB-330 cells (Fig. 5D). This is consistent with our observed interaction between the ERBB3:ERBB2 dimer and PIK3R2 (Fig. 2D), and the six high-affinity binding sites for phosphatidylinositol 3-kinase (PI3K)–p85 within ERBB3 (*48*–*50*). This ability of ERBB3:ERBB2 heterodimers to promote signaling through AKT is thought to drive oncogenic PI3K pathway activation in breast cancer (*51*). Through the application of our novel BiCAP technique, we have now demonstrated an additional and specific role for this heterodimer in the activation of ERK signaling and cell proliferation through a GRB2-FAM59A signaling axis.

DISCUSSION

The EGFR family members have been the subject of intensive research for the last few decades, although to date no method has allowed the sensitive and accurate discrimination of dimer-specific interactomes. Application of BiCAP to characterize the interactomes of the ERBB2 homodimer and heterodimers with EGFR and ERBB3 has overcome a number of limitations in existing approaches and revealed that although they share a core

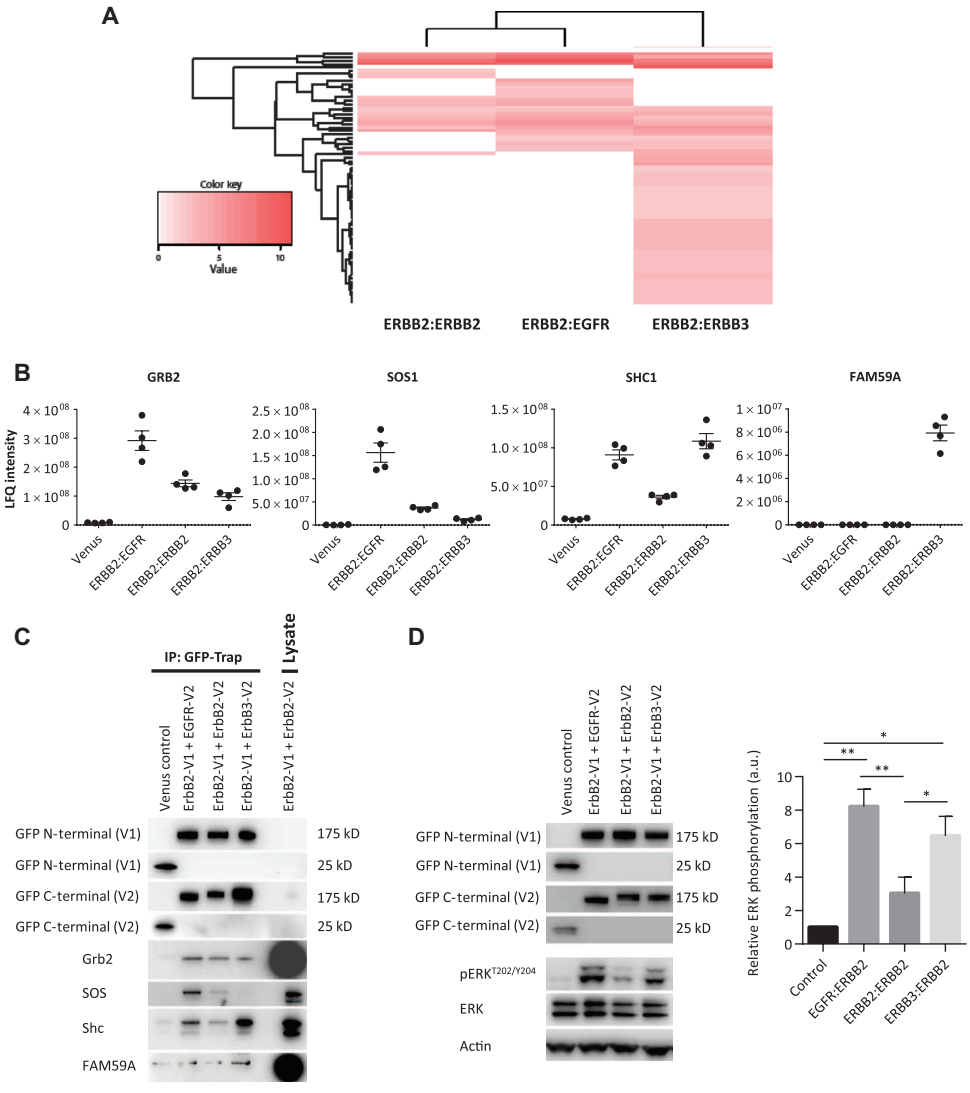

Fig. 4. Quantitative analysis and validation of diversity in ERBB2 dimer interactomes. (A) Heat map showing the interaction of proteins with either EGFR:ERBB2, ERBB2:ERBB2, or ERBB3:ERBB2, relative to the Venus control. (B) Label-free quantification (LFQ) of the interaction between each receptor dimer and the indicated proteins. Data are means ± SD, $n = 4$ experiments. (C) Western blotting validation for the coimmunoprecipitation of the indicated proteins in lysates from HEK-293T cells transfected with either a control plasmid or a combination of ERBB2-V1 and EGFR-V2, ERBB2-V2, or ERBB3-V2. Blots are representative of three experiments. (D) Western blotting for pERK$^{T202/Y204}$ and total ERK in lysates from cells transfected as in (C). Densitometry is normalized to actin. Data are means ± SD, $n = 3$ independent replicates. $^{*}P < 0.05$, $^{**}P < 0.01$, unpaired t test. a.u., arbitrary units.

group of interacting proteins, each receptor pair also has a unique repertoire of individual binding partners. The identification of this expected core group of proteins validates the BiCAP approach, although one unexpected omission from this core group is the adaptor protein GRB7, which is known to bind with high affinity to ERBB2 through its SH2 domain (*52*). Although GRB7 and ERBB2 are coamplified and coexpressed in some tumor types (*53*), the use of a HEK-293T transfection model in this study may have precluded the identification of this particular interaction.

Each of these receptors in isolation is potentially capable of binding a diverse set of interacting proteins, the most thoroughly characterized being the SH2 and PTB domain–containing proteins that are recruited by an array of different phosphosites on each receptor (*48*, *49*). This type of motif-based analysis is broadly consistent with the interactions that we observed for GRB2 but not for interactions with SHC1. We detected a much higher level of GRB2 binding by the EGFR:ERBB2 heterodimer than the ERBB2 homodimer or ERBB3:ERBB2 heterodimer, consistent with motif analysis, which predicts that EGFR has six GRB2-binding sites, ERBB2 has only one, and ERBB3 has two (*48*). However, this correlation is not apparent when considering SHC1 binding; both EGFR:ERBB2 and ERBB3:ERBB2 heterodimers bind substantially more SHC1 than the ERBB2 homodimer, even though EGFR has six predicted SHC1 binding sites, whereas ERBB2 has five and ERBB3 has only one (*48*). These conflicting observations highlight the limitation of motif-based interaction analysis in isolation, whereas the binding capacity of protein dimers in vivo may be heavily influenced by a combination of orthogonal factors.

Although relative interaction ratios may not be accurately predicted by motif-based analysis alone, the promiscuous nature of ERBB3:ERBB2 dimers has been previously inferred from this method (*49*). However, our BiCAP data now confirm this promiscuity with experimental data obtained using a technique that can specifically isolate and directly compare these dimers. The oncogenicity of receptor dimers within the EGFR family has been shown to be relative to their promiscuity in binding partners (*49*), consistent with the observation that ERBB2:ERBB3 has the most potent transforming capacity (*2*, *39*, *54*). This increased binding capability of the ERBB3:ERBB2 dimer may be due to the unique C-terminal region of ERBB3, which has the lowest homology between members of the EGFR family (*48*), although, in this system, it also appears that the expanded repertoire of proteins interacting with ERBB3:ERBB2 may also be influenced by the differing subcellular localization of this heterodimer (Fig. 2A).

The ability of the ERBB3:ERBB2 heterodimer to activate AKT signaling is well established (*50*), although from the intersection of our novel interactomics approach and biochemical assays in breast cancer cells we have now unveiled an additional, noncanonical, SOS-independent mechanism of ERK activation for this heterodimer that relies on FAM59A. In addition to our study, previous proteomics studies have demonstrated that each of SOS1, SOS2, and FAM59A appears to interact with GRB2 in a constitutive manner (*44*), suggesting the existence of an unknown regulatory mechanism that potentially drives the association of

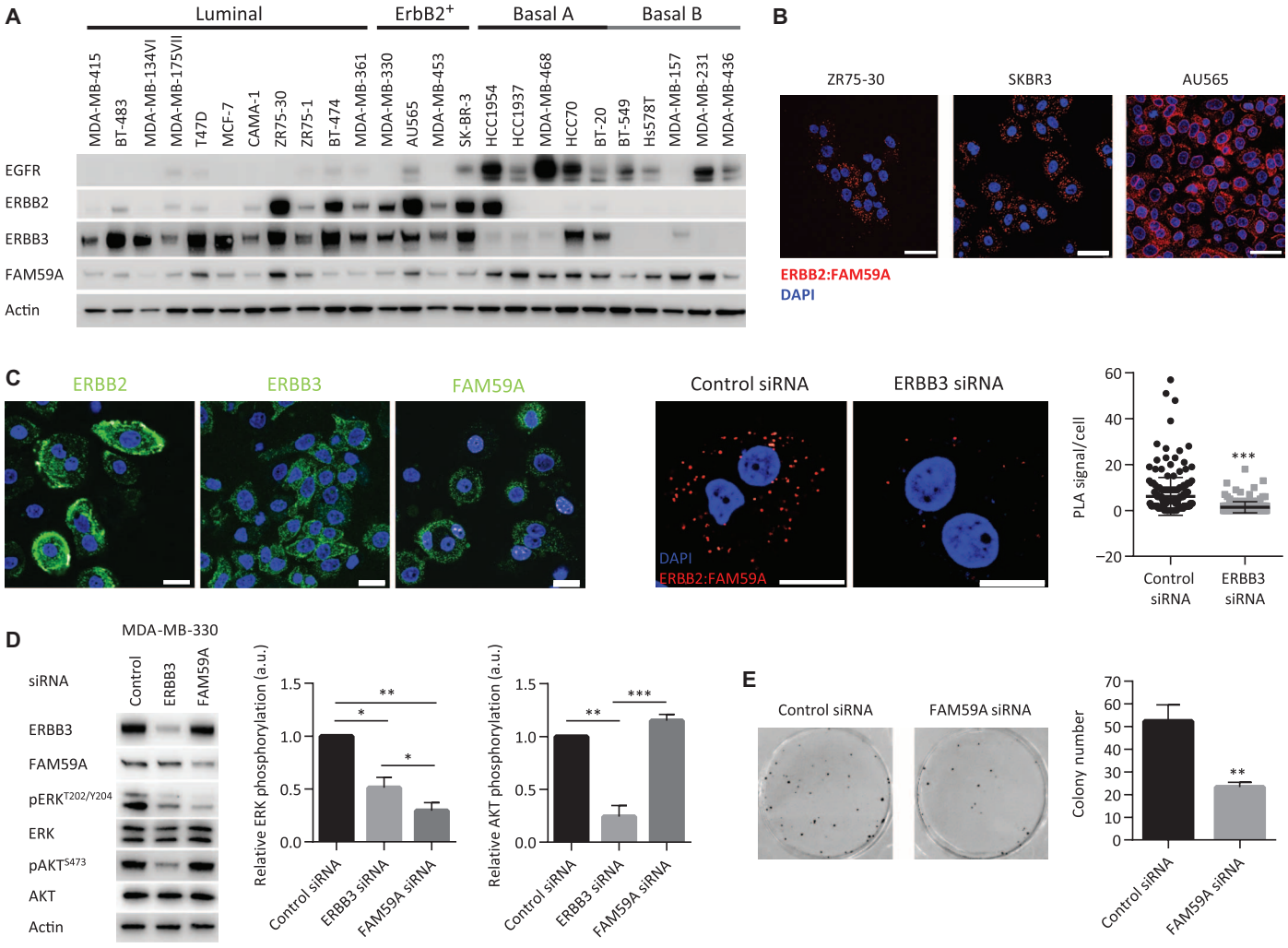

Fig. 5. FAM59A drives ERK activation downstream of the ERBB3:ERBB2 heterodimer in breast cancer cells. (**A**) Western blotting analysis of ERBB2, ERBB3, and FAM59A within a panel of 25 breast cancer cell lines, grouped by clinically defined subtype. Blots are representative of three experiments. (**B**) PLA validation of the ERBB2-FAM59A interaction in ZR75-30, SKBR3, and AU565 cell lines. Scale bar, 25 μm. Representative images from three independent experiments are shown. (**C**) Immunofluorescence of ERBB2, ERBB3, and FAM59A localization in MDA-MB-330 cells (left), and PLA analysis of the ERBB2 and FAM59A interaction in MDA-MB-330 cells treated with control or ERBB3 small interfering RNA (siRNA) (right). Scale bar, 20 μm. Data are means ± SD; $n = 200$ cells (100 cells for each condition from two independent experiments). $^{***}P < 0.001$, unpaired t test. (**D**) Western blot analysis of $pERK^{T202/Y204}$ and $pAKT^{S473}$ in MDA-MB-330 cells treated with siRNA targeting *ERBB3* or *FAM59A* (or control). Densitometry is normalized to actin. Data are means ± SD, $n = 3$ independent replicates. (**E**) Colony-forming assay in MDA-MB-330 cells after treatment with siRNA targeting FAM59A (or control). Data are means ± SD, $n = 3$ independent replicates. $^{*}P < 0.05$, $^{**}P < 0.01$, $^{***}P < 0.001$, unpaired t test.

mutually exclusive GRB2 signaling complexes with each specific receptor dimer.

The development of our novel BiCAP technique has allowed us to demonstrate the remarkable diversity of proteins interacting with different ERBB2-containing receptor dimers. We also identified a novel determinant of dimer-specific ERBB2 signaling, which may be relevant to understanding acquired resistance to therapeutics targeting these breast cancer oncogenes. The ability of BiCAP to specifically isolate and analyze protein complexes therefore represents an important advance in our ability to dissect and functionally characterize specific signaling complexes in a variety of cellular contexts.

MATERIALS AND METHODS

Antibodies, plasmids, and reagents

Antibodies against total ERBB2 (#2165), total EGFR (#4267), total ERBB3 (#12780), total ERK (#9201), total AKT (#9272), phospho-$ERK^{T202/Y204}$ (#4370), phospho-AKT^{S473} (#4060), AIFM1 (#5318), and GM130 (#12480) were from Cell Signaling. C-terminal GFP monoclonal antibody (11814460001) was from Roche, and N-terminal GFP monoclonal antibody (MMS-118P) was from Covance. The actin monoclonal (AC-15) and RAE1 polyclonal (R2905) antibodies were from Sigma-Aldrich, Shc antibody was from Calbiochem (ST1033), Grb2 antibody was from Santa

Cruz Biotechnology (sc-8034), FAM59A antibody was from Novus Biologicals (NBP2-24573), and SOS antibody was from Abcam (ab64595).

pDEST-V1 (Addgene plasmid 73637) and pDEST-V2 (Addgene plasmid 73638) vectors were assembled from various recombinant and synthetic components as described in fig. S7. pDONR223-EGFR (Addgene plasmid 23935), pDONR223-ERBB2 (Addgene plasmid 23888), and pDONR223-ERBB3 (Addgene plasmid 23874) constructs (*55*) were gifts from W. Hahn (Dana-Farber Cancer Institute) and D. Root (Broad Institute). Vectors expressing V1- or V2-labeled fusions of ERBB2, EGFR, or ERBB3 were generated by recombination cloning into pDEST-V1 or pDEST-V2 destination vectors using Gateway LR Clonase enzyme mix (Life Technologies) according to the manufacturer's instructions and verified by sequencing. An expression vector encoding full-length Venus fluorescent protein was a gift from S. Michnick (University of Montreal). siRNA toward ERBB3 (6504) was from Cell Signaling Technology. siRNA toward FAM59A was from Santa Cruz Biotechnology (#1-sc-77308) and Dharmacon (#2-L-013741-02-0005). Plasmid and siRNA transfection was performed using jetPRIME (Polyplus Transfection) according to the manufacturer's instructions.

Cell lines

The HEK-293T cell line was cultured in Dulbecco's modified Eagle's medium containing 10% fetal calf serum under standard tissue culture conditions (5% CO_2, 20% O_2). All breast cancer cell lines were obtained from the American Type Culture Collection, except for the MDA-MB-231 and T-47D lines (EG&G Mason Research Institute) and MCF-7 line (Michigan Cancer Foundation). Cell lines were authenticated by short tandem repeat polymorphism, single-nucleotide polymorphism, and fingerprint analyses, passaged for less than 6 months, and cultured as previously described (*56*). Colony formation assays were performed as previously described (*57*).

Western blotting and immunoprecipitation

Lysates for Western blotting and immunoprecipitation were prepared using normal lysis buffer [50 mM tris-HCl (pH 7.4), 150 mM NaCl, 1 mM EDTA, 1% (v/v) Triton X-100] containing protease inhibitor cocktail (p8340, Sigma) and 0.2 mM sodium orthovanadate. Immunoprecipitation was performed using either GFP-Trap_A (ChromoTek) or Protein G agarose beads (Invitrogen) as previously described (*58*). SDS–polyacrylamide gel electrophoresis (SDS-PAGE) and Western blotting were performed using the NuPAGE SDS-PAGE Gel System and NuPAGE Bis-Tris Precast Gels (4 to 12%) (Life Technologies). Western Lightning Plus-ECL, Enhanced Chemiluminescent Substrate (PerkinElmer) was used for imaging Western blots on the Vilber Lourmat Fusion chemiluminescent imaging system.

Confocal microscopy

HEK-293T cells were grown on glass coverslips, transfected with 500 ng of each BiFC construct, and incubated for 16 hours under standard tissue culture conditions. The coverslips were prepared for confocal microscopy by fixation with 1% paraformaldehyde for 5 min at room temperature, followed by permeabilization with phosphate-buffered saline (PBS) containing 1% Triton X-100 for 5 min at room temperature. For direct visualization, the cells were counterstained with DAPI for 5 min, followed by mounting with Mowiol mounting medium. For antibody staining, the cells were blocked with PBS containing 3% bovine serum albumin (BSA) for 30 min at room temperature, followed by staining with the primary antibody (1:200) and Cy5-labeled secondary antibody (1:1000), both in PBS containing 1% BSA. The cells were then counterstained with DAPI for 5 min, followed by mounting with Mowiol mounting medium. The PLA was performed using the Duolink In Situ Red Starter Kit, according to the manufacturer's instructions. Images were collected using the Leica DMI 6000 SP8 confocal microscope and analyzed using the particle analysis function of ImageJ.

Preparation of cell lysates for MS

HEK-293T cells were grown in 10-cm dishes and transfected with 2.5 μg of each BiFC construct. Cells were harvested by washing twice with warm PBS and then scraping on ice with ice-cold lysis buffer [50 mM tris-HCl (pH 7.4), 150 mM NaCl, 1 mM EDTA, 1% (v/v) Triton X-100] supplemented with fresh EDTA-free protease inhibitor cocktail and 0.2 mM sodium orthovanadate. Lysed cells were transferred to prechilled microcentrifuge tubes and incubated for 10 min on ice. Samples were cleared by centrifugation at 18,000*g* for 10 min at 4°C to remove cellular debris. Cleared supernatant was transferred to fresh microcentrifuge tubes and stored at −20°C for short-term storage or −80°C for long-term storage. Total protein concentration was determined by Bradford assay using Bio-Rad Protein Assay Dye Reagent Concentrate (Bio-Rad Laboratories)according to the manufacturer's instructions.

GFP-Trap affinity purification

BiFC dimers (or Venus alone as a negative control for nonspecific interactions) were affinity-purified from transfected HEK-293T cell lysates (in quadruplicate) using GFP-Trap_A agarose beads (ChromoTek GmbH) according to the manufacturer's protocol. Briefly, 1 mg of total lysate was incubated with 35 μl of GFP-Trap_A agarose bead slurry for 2 hours at 4°C with end-to-end rotation. Beads were extensively washed [10 mM tris-Cl (pH 7.5), 150 mM NaCl, 0.5 mM EDTA].

Trypsin digest and peptide desalting

GFP-Trap–bound proteins were digested on-bead with trypsin as previously described (*59*). Briefly, bound proteins were trypsinized in 60 μl of Buffer 1 [2 M urea, 50 mM tris-HCl (pH 7.5), trypsin (5 μg/ml)] for 30 min at 27°C in a thermomixer shaking at 800 rpm. Trypsin-digested beads were briefly centrifuged, and the supernatant was collected into fresh LoBind microcentrifuge tubes. Beads were then washed twice in 25 μl of Buffer 2 [2 M urea, 50 mM tris-HCl (pH 7.5), 1 mM dithiothreitol], and the supernatants were pooled with the trypsin digest. Pooled trypsin digest was incubated overnight at room temperature to continue digestion. The following day, 20 μl of iodoacetamide (5 mg/ml) (Life Science, Sigma-Aldrich, GmbH) was added to the trypsin digest and incubated for 30 min in the dark. Digested peptides were acidified with 1 μl of trifluoroacetic acid (TFA) (Fluka BioChemika, Sigma-Aldrich, GmbH) to inhibit trypsin and to acidify peptides for C18 StageTip desalting. C18 StageTips were constructed by stacking six layers of 3M Empore solid phase extraction C18 (Octadecyl) membrane with a total binding capacity of 30 μg (3M; Agilent Technologies) into a 200-μl micropipette tip. C18 StageTips were prepared by wetting with methanol (Vetec Fine Chemicals), equilibration with 0.1% (v/v) TFA, 80% (v/v) acetonitrile optima LC/MS (MeCN) (Fisher Scientific), followed by washes with 0.1% (v/v) TFA. Acidified peptides were loaded onto the C18 StageTips and then washed with 0.1% (v/v) TFA. Peptides were eluted using a two-step elution with 0.1% (v/v) TFA, 80% (v/v) MeCN and then dried using a vacuum concentrator. Dried peptides were stored at −80°C.

NanoLC-MS/MS

Desalted peptides were resuspended in 5% (v/v) formic acid, carefully loaded onto an LC plate, and placed into an EASY-nLC system (Thermo Scientific). Peptides were loaded onto a 20-cm column with a 75-μm inner diameter, packed in-house with 1.9 μm C18 ReproSil particles (Dr. Maisch GmbH). Peptides were eluted using a linear gradient of acetonitrile at 250 nl/min over 140 min. The EASY-nLC system was connected to an Orbitrap Velos Pro mass spectrometer (Thermo Fisher Scientific) with a nanospray source. Positive ions were generated using electrospray and the Orbitrap operated in data-dependent acquisition mode. Up to the 10 most abundant ions with charge states >+2 were sequentially isolated and fragmented within the

linear ion trap using higher-energy collisional dissociation. The mass/charge (*m/z*) ratios selected for MS/MS were dynamically excluded for 30 s.

MaxQuant software version 1.2.7.4 (*60*) was used to process raw MS data (using default settings; tables S1 and S2). The Andromeda search engine integrated into MaxQuant was used for database searching against the UniProt Human_11_2013 database (*61*). FDRs for protein, peptide, and sites were controlled at a maximum of 1%, and one missed cleavage was tolerated. Data analyses were performed using a modified statistical analysis workflow based on Perseus analysis workflow in the R software environment (*60*, *62*, *63*). Briefly, LFQ intensities of proteins identified using MaxQuant were transformed and filtered followed by normalization and imputation before statistical analysis to identify interacting proteins of each dimer pair by comparison with Venus control to exclude nonspecific background binders using Student's *t* test and Benjamini-Hochberg correction for multiple comparisons (analysis workflow is summarized in fig. S8 and complete data set is in table S3) (*60*). Nonunique peptides corresponding to highly conserved regions of EGFR and ERBB2 were excluded. Data quality was confirmed by comparison of individual histograms, multiple regression, and hierarchical clustering. Data were deposited into the ProteomeXchange database (accession PXD004148).

Functional pathway analysis

Gene names of BiFC dimer–interacting proteins were loaded into String (v9) protein interaction database (*64*). An interaction network was generated, which showed all known protein-protein interactions based on experimental evidence (excluding computational predictions) with a confidence score of 0.7 (high). The interaction network was imported into Cytoscape (*65*) for visualization and further analysis.

SUPPLEMENTARY MATERIALS

www.sciencesignaling.org/cgi/content/full/9/436/ra69/DC1
Fig. S1. BiFC detection of ERBB2 dimers.
Fig. S2. BiFC analysis of ERBB3:ERBB2 heterodimer and costaining with an antibody toward the Golgi body marker GM-130.
Fig. S3. Validation of novel interactors from MS data.
Fig. S4. ERBB2 coimmunoprecipitation of ERBB3.
Fig. S5. PLA controls.
Fig. S6. Validation of FAM59A knockdown in SKBR3 cells.
Fig. S7. BiFC vector construction.
Fig. S8. Pegasus statistical analysis workflow.
Table S1. MaxQuant parameters.
Table S2. MaxQuant output.
Table S3. LFQ proteomics analysis of ERBB2 dimer interactomes isolated by BiCAP.
Reference (*66*)

REFERENCES AND NOTES

1. T. Pawson, M. Kofler, Kinome signaling through regulated protein–protein interactions in normal and cancer cells. *Curr. Opin. Cell Biol.* **21**, 147–153 (2009).
2. W. Kolch, A. Pitt, Functional proteomics to dissect tyrosine kinase signalling pathways in cancer. *Nat. Rev. Cancer* **10**, 618–629 (2010).
3. C. Choudhary, M. Mann, Decoding signalling networks by mass spectrometry-based proteomics. *Nat. Rev. Mol. Cell Biol.* **11**, 427–439 (2010).
4. Y. Zheng, C. Zhang, D. R. Croucher, M. A. Soliman, N. St-Denis, A. Pasculescu, L. Taylor, S. A. Tate, W. R. Hardy, K. Colwill, A. Y. Dai, R. Bagshaw, J. W. Dennis, A. C. Gingras, R. J. Daly, T. Pawson, Temporal regulation of EGF signalling networks by the scaffold protein Shc1. *Nature* **499**, 166–171 (2013).
5. C. Jørgensen, M. Locard-Paulet, Analysing signalling networks by mass spectrometry. *Amino Acids* **43**, 1061–1074 (2012).
6. I. Rubin, Y. Yarden, The basic biology of HER2. *Ann. Oncol.* **12** (Suppl. 1), S3–S8 (2001).
7. H. S. Earp, T. L. Dawson, X. Li, H. Yu, Heterodimerization and functional interaction between EGF receptor family members: A new signaling paradigm with implications for breast cancer research. *Breast Cancer Res. Treat.* **35**, 115–132 (1995).
8. Y. Yarden, M. X. Sliwkowski, Untangling the ErbB signalling network. *Nat. Rev. Mol. Cell Biol.* **2**, 127–137 (2001).
9. D. J. Riese II, D. F. Stern, Specificity within the EGF family/ErbB receptor family signaling network. *BioEssays* **20**, 41–48 (1998).
10. D. J. Riese II, T. M. van Raaij, G. D. Plowman, G. C. Andrews, D. F. Stern, The cellular response to neuregulins is governed by complex interactions of the erbB receptor family. *Mol. Cell. Biol.* **15**, 5770–5776 (1995).
11. R. Worthylake, L. K. Opresko, H. S. Wiley, ErbB-2 amplification inhibits down-regulation and induces constitutive activation of both ErbB-2 and epidermal growth factor receptors. *J. Biol. Chem.* **274**, 8865–8874 (1999).
12. D. Graus-Porta, R. R. Beerli, J. M. Daly, N. E. Hynes, ErbB-2, the preferred heterodimerization partner of all ErbB receptors, is a mediator of lateral signaling. *EMBO J.* **16**, 1647–1655 (1997).
13. H. Creedon, A. Byron, J. Main, L. Hayward, T. Klinowska, V. G. Brunton, Exploring mechanisms of acquired resistance to HER2 (human epidermal growth factor receptor 2)-targeted therapies in breast cancer. *Biochem. Soc. Trans.* **42**, 822–830 (2014).
14. V. D'Amato, L. Raimondo, L. Formisano, M. Giuliano, S. De Placido, R. Rosa, R. Bianco, Mechanisms of lapatinib resistance in HER2-driven breast cancer. *Cancer Treat. Rev.* **41**, 877–883 (2015).
15. W. Kolch, M. Halasz, M. Granovskaya, B. N. Kholodenko, The dynamic control of signal transduction networks in cancer cells. *Nat. Rev. Cancer* **15**, 515–527 (2015).
16. P. Cassonnet, C. Rolloy, G. Neveu, P.-O. Vidalain, T. Chantier, J. Pellet, L. Jones, M. Muller, C. Demeret, G. Gaud, F. Vuillier, V. Lotteau, F. Tangy, M. Favre, Y. Jacob, Benchmarking a luciferase complementation assay for detecting protein complexes. *Nat. Methods* **8**, 990–992 (2011).
17. F. Rossi, C. A. Charlton, H. M. Blau, Monitoring protein–protein interactions in intact eukaryotic cells by β-galactosidase complementation. *Proc. Natl. Acad. Sci. U.S.A.* **94**, 8405–8410 (1997).
18. T. J. Magliery, C. G. M. Wilson, W. Pan, D. Mishler, I. Ghosh, A. D. Hamilton, L. Regan, Detecting protein–protein interactions with a green fluorescent protein fragment reassembly trap: Scope and mechanism. *J. Am. Chem. Soc.* **127**, 146–157 (2005).
19. C.-D. Hu, T. K. Kerppola, Simultaneous visualization of multiple protein interactions in living cells using multicolor fluorescence complementation analysis. *Nat. Biotechnol.* **21**, 539–545 (2003).
20. M. H. Kubala, O. Kovtun, K. Alexandrov, B. M. Collins, Structural and thermodynamic analysis of the GFP:GFP-nanobody complex. *Protein Sci.* **19**, 2389–2401 (2010).
21. R.-H. Tao, I. N. Maruyama, All EGF(ErbB) receptors have preformed homo- and heterodimeric structures in living cells. *J. Cell Sci.* **121**(Pt. 19), 3207–3217 (2008).
22. D. Szklarczyk, A. Franceschini, S. Wyder, K. Forslund, D. Heller, J. Huerta-Cepas, M. Simonovic, A. Roth, A. Santos, K. P. Tsafou, M. Kuhn, P. Bork, L. J. Jensen, C. von Mering, STRING v10: Protein–protein interaction networks, integrated over the tree of life. *Nucleic Acids Res.* **43**, D447–D452 (2015).
23. E. J. Lowenstein, R. J. Daly, A. G. Batzer, W. Li, B. Margolis, R. Lammers, A. Ullrich, E. Y. Skolnik, D. Bar-Sagi, J. Schlessinger, The SH2 and SH3 domain-containing protein GRB2 links receptor tyrosine kinases to ras signaling. *Cell* **70**, 431–442 (1992).
24. K. S. Ravichandran, Signaling via Shc family adapter proteins. *Oncogene* **20**, 6322–6330 (2001).
25. N. Li, A. Batzer, R. Daly, V. Yajnik, E. Skolnik, P. Chardin, D. Bar-Sagi, B. Margolis, J. Schlessinger, Guanine-nucleotide-releasing factor hSos1 binds to Grb2 and links receptor tyrosine kinases to Ras signalling. *Nature* **363**, 85–88 (1993).
26. X. Zhang, K. A. Pickin, R. Bose, N. Jura, P. A. Cole, J. Kuriyan, Inhibition of the EGF receptor by binding of MIG6 to an activating kinase domain interface. *Nature* **450**, 741–744 (2007).
27. L. Fiorentino, C. Pertica, M. Fiorini, C. Talora, M. Crescenzi, L. Castellani, S. Alemà, P. Benedetti, O. Segatto, Inhibition of ErbB-2 mitogenic and transforming activity by RALT, a mitogen-induced signal transducer which binds to the ErbB-2 kinase domain. *Mol. Cell. Biol.* **20**, 7735–7750 (2000).
28. S. Anastasi, L. Fiorentino, M. Fiorini, R. Fraioli, G. Sala, L. Castellani, S. Alemà, M. Alimandi, O. Segatto, Feedback inhibition by RALT controls signal output by the ErbB network. *Oncogene* **22**, 4221–4234 (2003).
29. B. P. Liu, K. Burridge, Vav2 activates Rac1, Cdc42, and RhoA downstream from growth factor receptors but not β1 integrins. *Mol. Cell. Biol.* **20**, 7160–7169 (2000).
30. X. R. Bustelo, Vav family exchange factors: An integrated regulatory and functional view. *Small GTPases* **5**, 9 (2014).
31. T. Yuan, Y. Wang, Z. J. Zhao, H. Gu, Protein-tyrosine phosphatase PTPN9 negatively regulates ErbB2 and epidermal growth factor receptor signaling in breast cancer cells. *J. Biol. Chem.* **285**, 14861–14870 (2010).
32. V. Bertelsen, E. Stang, The mysterious ways of ErbB2/HER2 trafficking. *Membranes* **4**, 424–446 (2014).
33. Z. Lu, T. Hunter, Degradation of activated protein kinases by ubiquitination. *Annu. Rev. Biochem.* **78**, 435–475 (2009).
34. B. Margolis, N. Li, A. Koch, M. Mohammadi, D. R. Hurwitz, A. Zilberstein, A. Ullrich, T. Pawson, J. Schlessinger, The tyrosine phosphorylated carboxyterminus of the EGF receptor is a binding site for GAP and PLC-γ. *EMBO J.* **9**, 4375–4380 (1990).

35. K. Kowanetz, N. Crosetto, K. Haglund, M. H. H. Schmidt, C.-H. Heldin, I. Dikic, Suppressors of T-cell receptor signaling Sts-1 and Sts-2 bind to Cbl and inhibit endocytosis of receptor tyrosine kinases. *J. Biol. Chem.* **279**, 32786–32795 (2004).
36. N. Kozer, D. Barua, C. Henderson, E. C. Nice, A. W. Burgess, W. S. Hlavacek, A. H. A. Clayton, Recruitment of the adaptor protein Grb2 to EGFR tetramers. *Biochemistry* **53**, 2594–2604 (2014).
37. A. H. A. Clayton, S. G. Orchard, E. C. Nice, R. G. Posner, A. W. Burgess, Predominance of activated EGFR higher-order oligomers on the cell surface. *Growth Factors* **26**, 316–324 (2008).
38. J.-H. Shim, C. Xiao, M. S. Hayden, K. -Y. Lee, E. S. Trombetta, M. Pypaert, A. Nara, T. Yoshimori, B. Wilm, H. Erdjument-Bromage, P. Tempst, B. L. M. Hogan, I. Mellman, S. Ghosh, CHMP5 is essential for late endosome function and down-regulation of receptor signaling during mouse embryogenesis. *J. Cell Biol.* **172**, 1045–1056 (2006).
39. M. Alimandi, A. Romano, M. C. Curia, R. Muraro, P. Fedi, S. A. Aaronson, P. P. Di Fiore, M. H. Kraus, Cooperative signaling of ErbB3 and ErbB2 in neoplastic transformation and human mammary carcinomas. *Oncogene* **10**, 1813–1821 (1995).
40. T. Funayama, T. Nakanishi, K. Takahashi, S. Taniguchi, M. Takigawa, T. Matsumura, Overexpression of c-erbB-3 in various stages of human squamous cell carcinomas. *Oncology* **55**, 161–167 (1998).
41. N. V. Sergina, M. Rausch, D. Wang, J. Blair, B. Hann, K. M. Shokat, M. M. Moasser, Escape from HER-family tyrosine kinase inhibitor therapy by the kinase-inactive HER3. *Nature* **445**, 437–441 (2007).
42. R. I. Cordo Russo, W. Béguelin, M. C. Díaz Flaqué, C. J. Proietti, L. Venturutti, N. Galigniana, M. Tkach, P. Guzmán, J. C. Roa, N. A. O'Brien, E. H. Charreau, R. Schillaci, P. V. Elizalde, Targeting ErbB-2 nuclear localization and function inhibits breast cancer growth and overcomes trastuzumab resistance. *Oncogene* **34**, 3413–3428 (2015).
43. U. Vijapurkar, K. Cheng, J. G. Koland, Mutation of a Shc binding site tyrosine residue in ErbB3/HER3 blocks heregulin-dependent activation of mitogen-activated protein kinase. *J. Biol. Chem.* **273**, 20996–21002 (1998).
44. N. Bisson, D. A. James, G. Ivosev, S. A. Tate, R. Bonner, L. Taylor, T. Pawson, Selected reaction monitoring mass spectrometry reveals the dynamics of signaling through the GRB2 adaptor. *Nat. Biotechnol.* **29**, 653–658 (2011).
45. K. Tashiro, T. Tsunematsu, H. Okubo, T. Ohta, E. Sano, E. Yamauchi, H. Taniguchi, H. Konishi, GAREM, a novel adaptor protein for growth factor receptor-bound protein 2, contributes to cellular transformation through the activation of extracellular signal-regulated kinase signaling. *J. Biol. Chem.* **284**, 20206–20214 (2009).
46. T. Taniguchi, S. Tanaka, A. Ishii, M. Watanabe, N. Fujitani, A. Sugeo, S. Gotoh, T. Ohta, M. Hiyoshi, H. Matsuzaki, N. Sakai, H. Konishi, A brain-specific Grb2-associated regulator of extracellular signal-regulated kinase (Erk)/mitogen-activated protein kinase (MAPK) (GAREM) subtype, GAREM2, contributes to neurite outgrowth of neuroblastoma cells by regulating Erk signaling. *J. Biol. Chem.* **288**, 29934–29942 (2013).
47. M. A. Smith, R. Hall, K. Fisher, S. M. Haake, F. Khalil, M. B. Schabath, V. Vuaroqueaux, H.-H. Fiebig, S. Altiok, Y. A. Chen, E. B. Haura, Annotation of human cancers with EGFR signaling–associated protein complexes using proximity ligation assays. *Sci. Signal.* **8**, ra4 (2015).
48. W. X. Schulze, L. Deng, M. Mann, Phosphotyrosine interactome of the ErbB-receptor kinase family. *Mol. Syst. Biol.* **1**, 2005.0008 (2005).
49. R. B. Jones, A. Gordus, J. A. Krall, G. MacBeath, A quantitative protein interaction network for the ErbB receptors using protein microarrays. *Nature* **439**, 168–174 (2006).
50. S. P. Soltoff, K. L. Carraway III, S. A. Prigent, W. G. Gullick, L. C. Cantley, ErbB3 is involved in activation of phosphatidylinositol 3-kinase by epidermal growth factor. *Mol. Cell. Biol.* **14**, 3550–3558 (1994).
51. T. Holbro, R. R. Beerli, F. Maurer, M. Koziczak, C. F. Barbas III, N. E. Hynes, The ErbB2/ErbB3 heterodimer functions as an oncogenic unit: ErbB2 requires ErbB3 to drive breast tumor cell proliferation. *Proc. Natl. Acad. Sci. U.S.A.* **100**, 8933–8938 (2003).
52. P. W. Janes, M. Lackmann, W. B. Church, G. M. Sanderson, R. L. Sutherland, R. J. Daly, Structural determinants of the interaction between the erbB2 receptor and the Src homology 2 domain of Grb7. *J. Biol. Chem.* **272**, 8490–8497 (1997).
53. A. Walch, K. Specht, H. Braselmann, H. Stein, J. R. Siewert, U. Hopt, H. Höfler, M. Werner, Coamplification and coexpression of GRB7 and ERBB2 is found in high grade intraepithelial neoplasia and in invasive Barrett's carcinoma. *Int. J. Cancer* **112**, 747–753 (2004).
54. C. Wallasch, F. U. Weiss, G. Niederfellner, B. Jallal, W. Issing, A. Ullrich, Heregulin-dependent regulation of HER2/neu oncogenic signaling by heterodimerization with HER3. *EMBO J.* **14**, 4267–4275 (1995).
55. C. M. Johannessen, J. S. Boehm, S. Y. Kim, S. R. Thomas, L. Wardwell, L. A. Johnson, C. M. Emery, N. Stransky, A. P. Cogdill, J. Barretina, G. Caponigro, H. Hieronymus, R. R. Murray, K. Salehi-Ashtiani, D. E. Hill, M. Vidal, J. J. Zhao, X. Yang, O. Alkan, S. Kim, J. L. Harris, C. J. Wilson, V. E. Myer, P. M. Finan, D. E. Root, T. M. Roberts, T. Golub, K. T. Flaherty, R. Dummer, B. L. Weber, W. R. Sellers, R. Schlegel, J. A. Wargo, W. C. Hahn, L. A. Garraway, COT drives resistance to RAF inhibition through MAP kinase pathway reactivation. *Nature* **468**, 968–972 (2010).
56. M. T. Herrera Abreu, W. E. Hughes, K. Mele, R. J. Lyons, D. Rickwood, B. C. Browne, H. L. Bennett, P. Vallotton, T. Brummer, R. J. Daly, Gab2 regulates cytoskeletal organization and migration of mammary epithelial cells by modulating RhoA activation. *Mol. Biol. Cell* **22**, 105–116 (2011).
57. D. R. Croucher, D. Rickwood, C. M. Tactacan, E. A. Musgrove, R. J. Daly, Cortactin modulates RhoA activation and expression of Cip/Kip cyclin-dependent kinase inhibitors to promote cell cycle progression in 11q13-amplified head and neck squamous cell carcinoma cells. *Mol. Cell. Biol.* **30**, 5057–5070 (2010).
58. D. Fey, M. Halasz, D. Dreidax, S. P. Kennedy, J. F. Hastings, N. Rauch, A. G. Munoz, R. Pilkington, M. Fischer, F. Westermann, W. Kolch, B. N. Kholodenko, D. R. Croucher, Signaling pathway models as biomarkers: Patient-specific simulations of JNK activity predict the survival of neuroblastoma patients. *Sci. Signal.* **8**, ra130 (2015).
59. B. Turriziani, A. Garcia-Munoz, R. Pilkington, C. Raso, W. Kolch, A. von Kriegsheim, On-beads digestion in conjunction with data-dependent mass spectrometry: A shortcut to quantitative and dynamic interaction proteomics. *Biology* **3**, 320–332 (2014).
60. J. Cox, M. Mann, MaxQuant enables high peptide identification rates, individualized p.p.b.-range mass accuracies and proteome-wide protein quantification. *Nat. Biotechnol.* **26**, 1367–1372 (2008).
61. J. Cox, N. Neuhauser, A. Michalski, R. A. Scheltema, J. V. Olsen, M. Mann, Andromeda: A peptide search engine integrated into the MaxQuant environment. *J. Proteome Res.* **10**, 1794–1805 (2011).
62. S. Hogl, F. van Bebber, B. Dislich, P.-H. Kuhn, C. Haass, B. Schmid, S. F. Lichtenthaler, Label-free quantitative analysis of the membrane proteome of Bace1 protease knock-out zebrafish brains. *Proteomics* **13**, 1519–1527 (2013).
63. Y. Benjamini, Y. Hochberg, Controlling the false discovery rate: A practical and powerful approach to multiple testing. *J. R. Stat. Soc. B Methodol.* **57**, 289–300 (1995).
64. B. Snel, G. Lehmann, P. Bork, M. A. Huynen, STRING: A web-server to retrieve and display the repeatedly occurring neighbourhood of a gene. *Nucleic Acids Res.* **28**, 3442–3444 (2000).
65. P. Shannon, A. Markiel, O. Ozier, N. S. Baliga, J. T. Wang, D. Ramage, N. Amin, B. Schwikowski, T. Ideker, Cytoscape: A software environment for integrated models of biomolecular interaction networks. *Genome Res.* **13**, 2498–2504 (2003).
66. J. Cox, M. Mann, 1D and 2D annotation enrichment: A statistical method integrating quantitative proteomics with complementary high-throughput data. *BMC Bioinformatics* **13**, S12 (2012).

Acknowledgments: We would like to acknowledge W. Hahn and D. Root for provision of the pDONR223-EGFR, pDONR223-ERBB2, and pDONR223-ERBB3 plasmids. Expression vector encoding full-length Venus fluorescent protein was a gift from S. Michnick. **Funding:** D.R.C. is a Cancer Institute New South Wales (NSW) Fellow and D.N.S. was previously a Cancer Institute NSW Fellow. The research findings presented in this article were funded by the Cancer Institute NSW (13/FRL/1-02 and 09/CDF/2-39), the National Health and Medical Research Council (project grant GNT1052963), the Science Foundation Ireland (11/SIRG/B2157), the NSW Office of Science and Medical Research, the Guest Family Fellowship, and the Mostyn Family Foundation. M.I., J.F.H., and R.F.S. were recipients of an Australian Postgraduate Award. **Author contributions:** D.R.C. conceived the study, wrote and edited the manuscript, and performed experiments relating to coimmunoprecipitation, Western blotting, and signaling pathway analysis. D.R.C. also supervised J.F.H., J.Z.R.H., and S.P.K. M.I. performed the MS sample preparation, data acquisition, and data analysis. J.F.H. performed coimmunoprecipitation, Western blotting, and signaling pathway experiments and performed plasmid preparation. S.P.K. performed the confocal microscopy and PLAs. J.Z.R.H. performed coimmunoprecipitation, Western blotting, and signaling pathway experiments. J.M. assisted with MS data analysis. A.W., J.L., and R.F.S. assisted with experimental design and plasmid construction and validation. S.A. contributed to experimental design and analysis. D.N.S. conceived the study, performed structural and data analyses, wrote and edited the manuscript, and supervised M.I., J.M., and R.F.S. **Competing interests:** The authors declare that they have no competing interests. **Data and materials availability:** Data have been deposited to the ProteomeXchange database, accession ID PXD004148. Plasmids described in this article have been deposited with and will be available through Addgene under a standard materials transfer agreement.

Submitted 20 January 2016
Accepted 14 June 2016
Final Publication 12 July 2016
10.1126/scisignal.aaf0793
Citation: D. R. Croucher, M. Iconomou, J. F. Hastings, S. P. Kennedy, J. Z. R. Han, R. F. Shearer, J. McKenna, A. Wan, J. Lau, S. Aparicio, D. N. Saunders, Bimolecular complementation affinity purification (BiCAP) reveals dimer-specific protein interactions for ERBB2 dimers. *Sci. Signal.* **9**, ra69 (2016).

Bimolecular complementation affinity purification (BiCAP) reveals dimer-specific protein interactions for ERBB2 dimers

David R. Croucher, Mary Iconomou, Jordan F. Hastings, Sean P. Kennedy, Jeremy Z. R. Han, Robert F. Shearer, Jessie McKenna, Adrian Wan, Joseph Lau, Samuel Aparicio and Darren N. Saunders

(July 12, 2016)
Science Signaling **9** (436), ra69. [doi: 10.1126/scisignal.aaf0793]